551.557.5 : 551.513.1 : 608.4

A STUDY OF THE SYMMETRICAL GENERAL CIRCULATION BY THE AID OF A ROTATING WATER TANK EXPERIMENT*)

by

AIMO VÄISÄNEN

Institute of Meteorology, University of Helsinki

Abstract

The three-dimensional structure of the flow of water in a symmetrical dishpan experiment is computed and compared with the atmosphere. The zonal velocity distribution was observed at the top surface and also internally at some levels; in particular the height of the level at which the flow changes from an easterly direction near the bottom to a westerly one higher up, was determined. Observations showed almost strictly zonal symmetric flow with the meridional component one order smaller than the zonal component. Assuming the steady state it was possible to compute the whole field of the zonal velocity using the gradient wind equation. Two different methods were used in calculating the meridional winds. The angular momentum budget was computed. Also the balance of the kinetic energy and the release of free potential energy was examined. The most interesting result dealing with the angular momentum was the fact, that the fluid ignores the potentially greatest momentum source, the warm wall. RIEHL and FULTZ [9] have earlier arrived at the same conclusion for the three-wave case. The speed of the meridional motion and the location of the angular momentum sources and sinks agree fairly well with the theoretical meridional circulation model presented by ELIASSEN [2]. The energy considerations showed that at high Rossby numbers the magnitude of frictional relative to the other forces can became much greater than at low Rossby numbers.

*) This research was performed under contracts between the Office of Naval Research and The University of Chicago (Contract No. N6ori-02036 Project NR 082—120) while the writer was on leave of absence at The University of Chicago.

Introduction

Experiments made by FULTZ *et al* [4] in rotating dishpans have shown that in concentric cylinder arrangements three discrete regimes of water circulation are observed, depending on rotation and heating rates:

1) single, zonally symmetric general circulation
2) steady wave pattern with jet stream
3) unsteady wave patterns with jet stream, sometimes with repeating cycle.

The present investigation has been carried out to try and employ water circulation as an analogy for studying certain dynamical aspects of atmospheric wind currents. This type of approach has been followed by FULTZ *et al* [4], by RIEHL and FULTZ [8, 9] and others, who have analyzed various regimes in the dishpan from the viewpoint of comparability with the atmosphere. In particular, RIEHL and FULTZ [8] have studied a case containing three steady long waves and with jet stream; frequent reference to this paper will be made in the present article. Using nondimensional quantities, they have shown that considerable similarity exists between dishpan and atmospheric flow patterns in subtropical and middle latitudes: for instance the strength of the jet streams is almost the same in the relative frame. One of the most interesting results of these studies is the difference in general circulation mechanisms obtained when averaging is performed in two types of coordinate systems: conventional polar coordinates and a curvilinear system which follows the jet stream axis. The latter set of coordinates brings out in a clear manner the importance of thermally produced ageostrophic mass circulations in maintaining the observed flow and thermal structure.

The experiment to be described here has steady symmetrical westerly flow in upper levels, typical of the first regime mentioned. In such experiments, polar and curvilinear coordinate systems following the jet axis become identical because the jet stream is an almost zonal current. Analysis of two-dimensional cases may not have served in an important way the main purpose, which is to obtain insight into atmospheric motion through model experiments. The atmosphere is invariant neither in longitude nor time. However, the asymmetric part of the motion often consists in smooth long waves in the westerlies. In such cases, one can average following the jet stream and obtain cross sections representative of the symmetric part of the general circulation in the first approximation. Occasionally also, nearly zonal jet streams are observed. Averaging

such a current has been performed, for instance, by PALMÉN and NAGLER [5]; their results are compared with those obtained from the dishpan in the following.

ELIASSEN [2] has developed a model for slow, thermally and frictionally controlled meridional circulation in an axially symmetric vortex. He applied his deductions to the cross section of PALMÉN and NAGLER in trying to explain the possible meridional circulations. This model will also be examined further near the end of this paper.

Observations

The purpose of this study was to analyze a symmetric general circulation case in a manner similar to that of RIEHL and FULTZ [8] for the three-wave case. However, techniques of observations had, to some extent, been improved since the early experiment and a much denser network of observations was available in the dishpan, especially near the boundaries. This dense data was very helpful in computing quantities such as the momentum exchange between the pan and the water inside the pan.

The most important differences in apparatus of the present compared to the three-wave experiment were the following:

a) A pan with radius of 19.6 cm. was used, previously 15.6 cm. The radius of the central cylindrical cold source was 4.7 cm., preciously 6.5 cm. Water depth was 6 cm., previously 4 cm. The relative areas of warm and cold walls are not the same in both cases, a difference which has some influence on the temperature distribution.

b) The ratio of spacing between inner and outer walls to the mean radius of the annular ring contained between the walls was different. This has an influence on the velocity distribution and momentum balance.

c) In the three-wave experiment the warm wall was not vertical and the heat source extended around the rim and also inward along the bottom. In the present case the walls were vertical and the heat source insulated, so that heat conduction along the bottom of the pan was held to low values if indeed it existed at all. The cold source was operated by means of circulating cold water as in the earlier experiment. An identical method also was used in computing heat transport by the water in the annular ring from heat source to cold source; the temperature of the circulating water in the cold source was measured before it entered and after it left the cold source.

d) Evaporation from the pan into the atmosphere was diminished gretlay by a plastic cover. In one of two symmetrical regime experiments carried out, the evaporation cooling was estimated to have a rate of 6 watts, determined from the total water loss over the experiment. In the other, evaporation was so small that one could not measure it. Only this experiment will be considered in this paper. Taking into account all other factors affecting heat balance, the rate of heat abstraction through the cold wall was 81 watts in the first experiment, hence the effective strength of the heat source 87 watts, although the nominal strength was 100 watts. In the second case the direct radiative heat transfer to the atmosphere was even smaller, and the nominal heat source of 100 watts was found to decrease only to 94 watts by this means; as just stated, evaporation cooling was very small so that the heat transfer by the fluid can be taken as 94 watts. These instrumental improvements were the consequence of technical innovations in photography, etc., the details of which can be found in a report by FALLER [3].

Figs. 1 and 2 show the radial temperature distribution in the symmetrical cases analyzed. They clearly reveal the lack of evaporation in

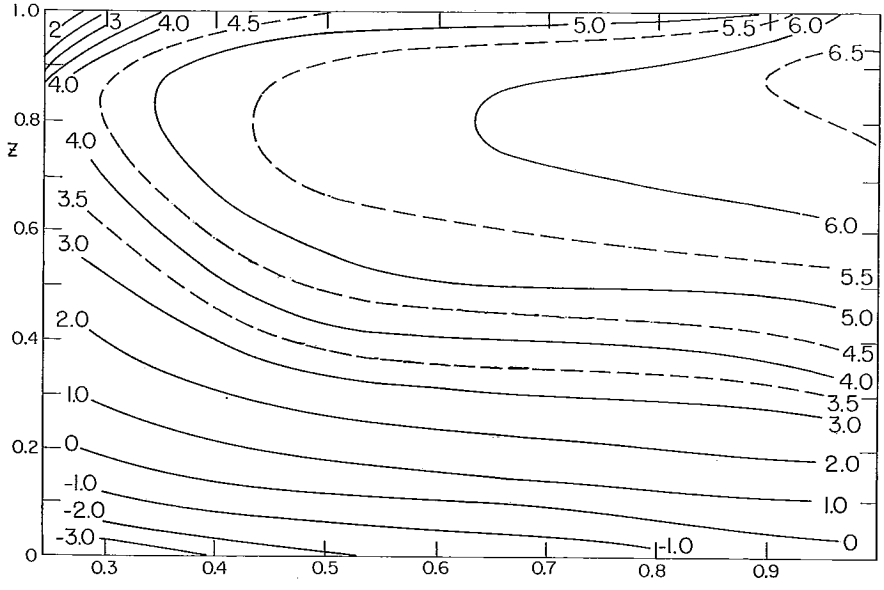

Fig. 1. Isotherms (°C, deviation from 22 °C) in $r' - z'$ plane in experiment with appreciable evaporation from top.

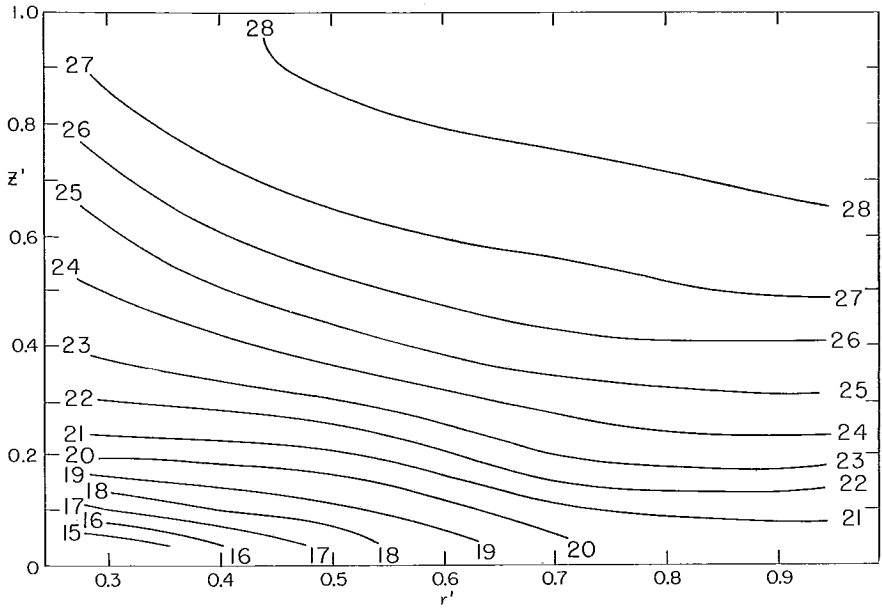

Fig. 2. Same as Fig. 1, with evaporation suppressed. (°C)

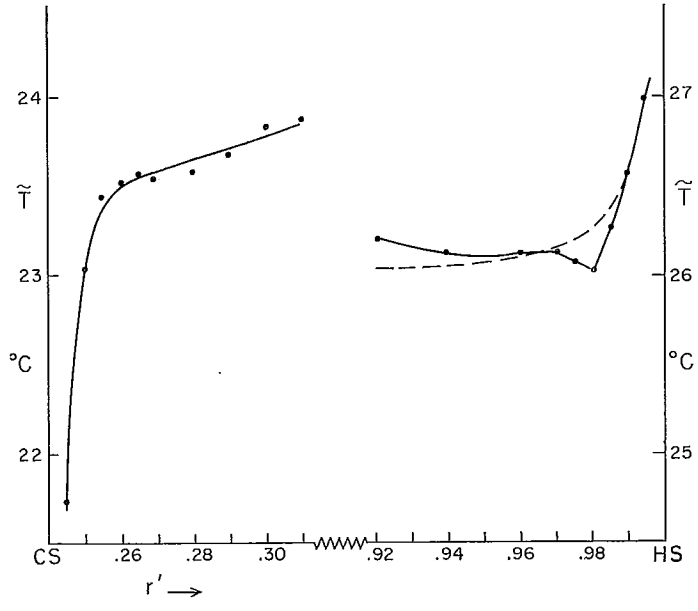

Fig. 3. Temperature observations in the boundary layers.

the second case, since temperature continued to increase to the top. Fig. 3 contains vertically averaged temperatures in the vicinity of heat and cold sources for the nonevaporating case. The radial gradient of mean temperature does not change enough for molecular transfer of heat to be effective in changing individual fluid temperatures except within 0.5 mm. from the cold source. In the interior of the water, heat transport by conduction is negligible, and we must assume that the ageostrophic mass circulation performs here the bulk of the lateral heat transport. Unfortunately, knowledge about the surface film is poor, but one can see from the vertical temperature distribution that, except near top and bottom, the stratification of the water is stable with a nearly linear lapse rate in the interior of the fluid. In the case of the first experiment with evaporation, the vertical temperature gradient reverses near the top, but near the bottom there is not as clear a convective regime as in the three-wave case where the heat source spread along the bottom. In the present case, as mentioned, this was prevented by insulation of the heat source. Nevertheless, the temperature of the bottom water increased somewhat during travel from cold to heat source before reaching the cold source, and it must be concluded that heat conduction from above takes place throughout the liquid and probably some from the bottom in the boundary layer.

Zonal Wind Component

We shall consider a cylindrical coordinate system (r, Θ, z) rotating at the same rate as the dishpan. The angle Θ is taken positive counterclockwise about the pole or the axis of the cylinder; r is positive outwards from the pole and z is positive upward. The velocity components along the three axes will be v_{or}, v, and v_z. Following the reasoning given by FULTZ [4] and others, we shall introduce nondimensional forms for distances and velocities as follows:

$s' \equiv s/r_0$ where r_0 is the radius of the pan
$z' \equiv z/r_0$
$c' \equiv c/c_e$, where $c_e = r_0\omega$, the equatorial speed of the pan, and ω is the rotation of the pan
$t' \equiv \omega t$.

It is the advantage of using such nondimensional quantities in calculations that the results can be compared with those of calculations made on rotating bodies with a different size or rate of rotation.

The zonal velocity distribution was measured at the top surface with methods discussed by FULTZ *et al* [4]. It was also measured internally; in particular the height of the level at which the flow changes from an easterly direction near the bottom to westerly higher up, was determined. These measurements were made with Tellurium probes (discussed more by FALLER [3]); the level without zonal motion was located from these about 1 cm. above the bottom without much scatter of the data points.

For determination of the complete wind distribution we shall use cylindrical equations of motion in the form:

$$\frac{dv_\theta'}{dt'} + \frac{v_\theta' v_r'}{r'} + f' v_r' = -\frac{1}{\varrho'}\frac{\partial p'}{r' \partial \theta} + \frac{1}{\varrho'}\frac{\partial \tau_{\theta z}'}{\partial z'} + \frac{1}{\varrho'}\frac{\partial \tau_{\theta r}'}{\partial r'} + \frac{2\tau_{\theta r}'}{\varrho' r'}, \tag{1}$$

$$\frac{dv_r'}{dt'} - \frac{v_\theta'^2}{r'} - f' v_\theta' = -\frac{1}{\varrho'}\frac{\partial p'}{\partial r'} + \left(\frac{1}{\varrho'}\frac{\partial \tau_{rz}'}{\partial z'} + \frac{1}{\varrho'}\frac{\partial \tau_{rr}'}{\partial r'} + \frac{1}{\varrho'}\frac{\tau_{rr}' - \tau_{\theta\theta}'}{r'}\right)^*. \tag{2}$$

The last terms on the right of (1) and (2) are correction terms arising from curvature of the cylindrical coordinate lines.

All photographs and measurements show almost strictly zonal symmetric flow. Observations of the meridional component indicate that, except for the bottom region, it is one order of magnitude smaller than the zonal component. The whole system may be considered to be in steady state for large-scale motion. The steady state assumption implies that we suppose the heat and angular momentum sources to be weak enough and to change with time slowly enough, so that we need not take into account forced oscillations which, with other assumptions, could occur in the meridional motion. Setting $dv_r/dt = 0$ and assuming that the frictional accelerations in the radial direction are small along with v_r, gradient wind balance prevails and the zonal component of motion can be determined given the distribution of pressure or height of isobaric surfaces. Solving the gradient wind equation for v_θ,

$$v_\theta = -r \pm \sqrt{r^2 - \frac{\partial(g\varrho z)}{\partial r}}, \tag{3}$$

where the hydrostatic assumption has been made.

In computing the geopotential $g\varrho z$, DORSEY's »*Properties of Ordinary Water Substance*» [1] has been used. From the observations the height of the level with zero zonal motion is known, so that the zonal wind field can be determined using the thermal wind assumption at all depths

* In the following the primes will often be omitted for simpler notation.

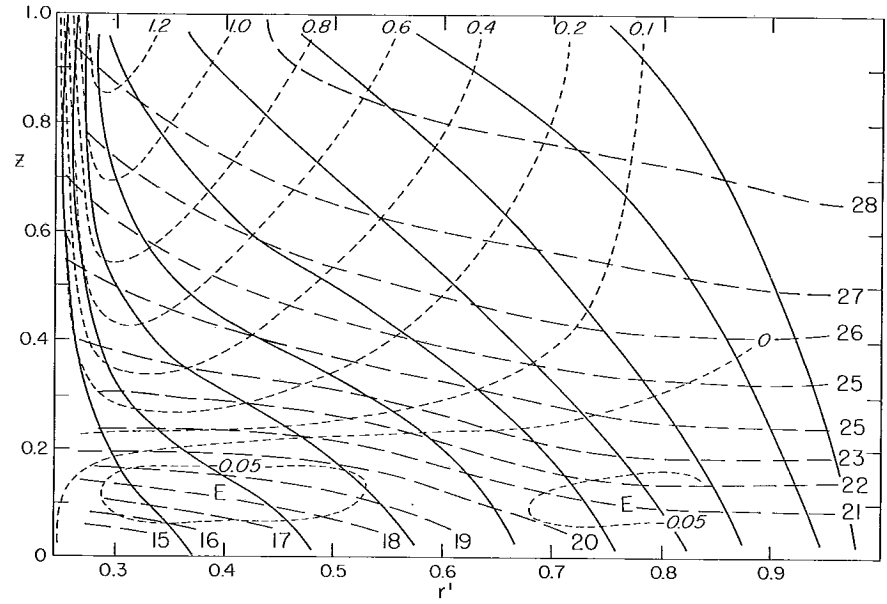

Fig. 4. Isolines of constant absolute angular momentum (solid), isotachs (short dashes) and isotherms (long dashes). *E* denotes easterlies.

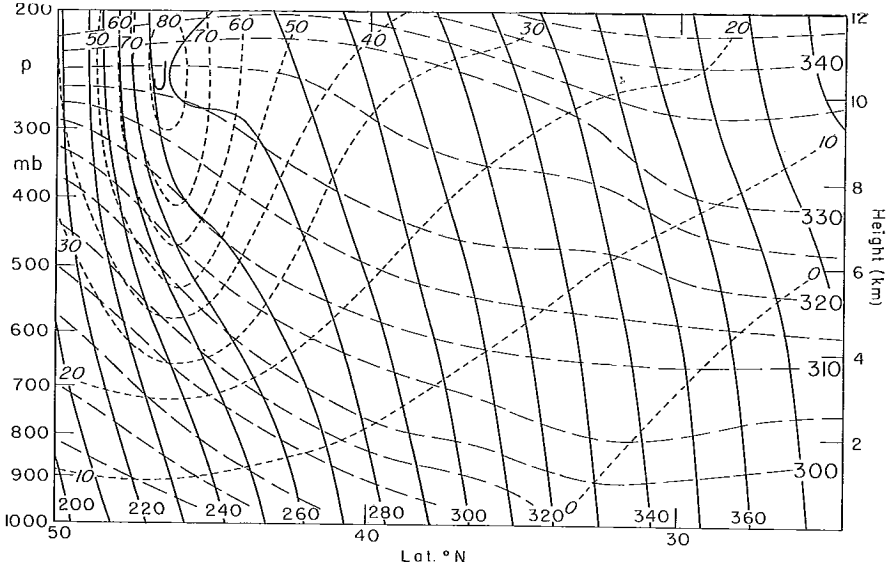

Fig. 5. Same as Fig. 4, for jet stream analyzed by PALMÉN and NAGLER [5].

(Fig. 4). Computed and observed velocities at the top surface were in excellent agreement. The jet stream is well marked and centered very close to the cold source. The kinematic Rossby number u/c_e is about 1.4 on the surface at the radius of strongest wind. In the three-wave case it was 0.2 in the jet, or seven times smaller, a consequence of much higher rate of pan rotation ($\omega = 0.3$ compared to $\omega = 0.05$ for the symmetric vortex). In the cross section of PALMÉN and NAGLER (Fig. 5), the Rossby number was about 0.17 in the jet. Such values in the atmosphere, very near those characteristic for the three-wave case, are typical for the atmosphere and show the dynamic similarity of asymmetric dishpan cases and the atmosphere.

The much higher Rossby number of the present experiment clearly brings out the fundamental difference between symmetric and asymmetric regimes. The asymmetric regime is nearly geostrophic whereas in the symmetric vortex the centrifugal acceleration v_θ^2/r has the same magnitude as the Coriolis acceleration fv_θ over considerable portions of the fluid.

Another important dynamical difference compared with the atmosphere is the fact the easterly flow is observed to extend across the entire bottom as on the three-wave experiment, so far as zonal averages are concerned.

Meridional Wind Component

It is much more difficult to determine the distribution of the small radial wind component v_r' than that of v_θ'. Direct measurements made at the free surface are of uncertain quality because of the surface film. Watching the experiment, one can see clearly that a very thin shearing layer existed at the top of the fluid, but it was difficult to make satisfactory observations of the magnitude of the shear. Fig. 6 shows the average distribution of v_r' from the observations made at the free surface. Evidently, the scatter is so large that the curve representing the average of all measurements cannot be considered reliable. The other curve in Fig. 6 represents the distribution of v_r', assuming that $v_r'r'$ is constant along the radius. Table 1 shows some of the values of v_r' measured in the interior of the fluid with Tellurium probes and dyes.

ELIASSEN's problem [2] was to compute the stream function of this slow meridional cell theoretically from fixed heat and angular momentum sources. Because of the ratio of horizontal and vertical scales and

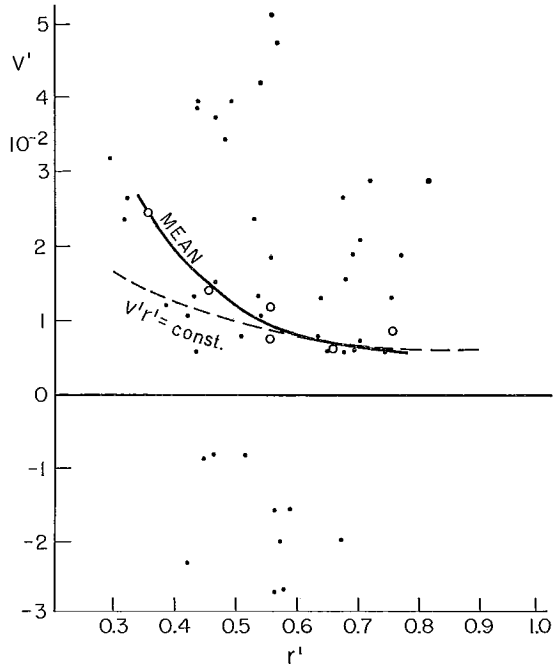

Fig. 6. Measured values of v_r' at top surface.

especially because of the frictional effect of the walls, the dishpan circulation may not be comparable with ELIASSEN's model. Hence the meridional circulation must be computed with methods different from assuming any particular model to hold, but it will be interesting to compare the dishpan results with those obtained by ELIASSEN.

For computing v_r several methods are available:

1. In the steady symmetric case the first equation of motion may be written

$$v_r \frac{\partial v_\theta}{\partial r} + v_z \frac{\partial v_\theta}{\partial z} + \frac{v_\theta v_r}{r} + f v_r = \nu \left(\nabla^2 v_\theta - \frac{v_\theta}{r^2} \right), \tag{4}$$

where the density has been taken as unity and ν is the kinematic coefficient of viscosity. Further, the equation for heat flow is

$$v_r \frac{\partial T}{\partial r} + v_z \frac{\partial T}{\partial z} = K \nabla^2 T , \tag{5}$$

where K is the coefficient of thermometric conductivity.

Eliminating v_z from equations (4) and (5),

$$v_r = \frac{\frac{\partial T}{\partial t} \nu \left(\nabla^2 v_\theta - \frac{v_\theta}{r^2} \right) - \frac{\partial v_\theta}{\partial z} K \nabla^2 T}{(f + \zeta) \frac{\partial T}{\partial z} - \frac{\partial T}{\partial r} \frac{\partial v_\theta}{\partial z}} . \tag{6}$$

This form of solution for v_r includes second derivatives of T and v_θ. Therefore it is very difficult to determine v_r in every portion of the cross section, especially in the zone of weak easterly winds. After interpolation for the areas with doubtful second derivatives (only $\partial^2 v_\theta / \partial z^2$ was retained) and introduction of the equation of mass continuity, Fig. 7 was obtained which represents the distribution of the Stokes' stream function for the meridional cell.

2. If the temperature field is known with a high degree of accuracy, the vector $\mathbf{v} = \vec{v}_r + \vec{v}_z$ can be evaluated directly from equation (5).

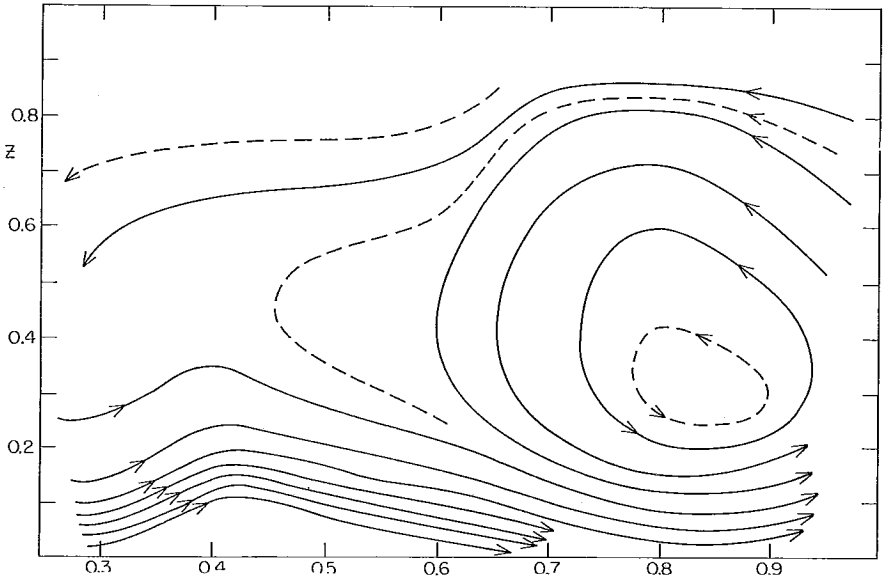

Fig. 7. Isolines of Stokes' stream function [computed from the expression $\bar{v}_r r = \frac{\partial \bar{\psi}}{\partial z}$, $\bar{\psi}_{i,j} = \psi_{i,j-1} + \frac{(v_{i,j+1} - v_{i,j-1}) r_i}{2 \Delta z_i}$] for the meridional velocities obtained from eq. (6).

This technique has been tried by FALLER [3] but has been found to be computationally unstable for derivatives.

3. Finally the method used by RIEHL and FULTZ [8, 9] was applied. Given a stationary temperature field and meridional heat flow at each radius, one can answer this question: what vertical profile of the radial flow will accomplish the heat transport if the kinetic energy of the meridional motion is to be held to a minimum. The solution is:

$$v_r' = KH_m' \frac{T^\circ}{\widetilde{T^{\circ 2}}} . \tag{7}$$

Here H_m' is the mean meridional heat flow, $\sim$ denotes vertical averaging, T° is departure from the vertically averaged temperature and K is a constant giving correct dimensions. In the steady three-wave case this method, which does not require knowlefge of v_r' anywhere, checked satisfactorily with observed values of v_r' near top and bottom.

The heat transport H across an arbitrary cylinder is:

$$H = 2\pi r \int_0^D (c_w T')\,(\varrho v_r) dz . \tag{8}$$

Further $H' = H/c_w \omega \varrho r_0^3$, and $H_m' = H/c_w r_0^3 \varrho \omega 2\pi r' D'$. Hence,

$$v_r' = \frac{H}{2\pi r' D' \varrho \omega c_w r_0^3} \frac{T^\circ}{\widetilde{T^{\circ 2}}} \tag{9}$$

when H is expressed in watts.

Evidently v_r' obtained with equation (6) is mostly smaller, and the kinetic energy of the radial motion integrated over the whole dishpan is also smaller than that computed from equation (9). The heat balance requirement, however, cannot be satisfied with these values. In the following we shall use the results of equation (9). Fig. 8 represents the Stokes' stream function from the minimum v_r' distribution after evaluation of v_z' from mass continuity. The vertical motion is concentrated very close to the heat and cold sources in the single »direct» cell depicted in Fig. 8.

Angular Momentum Budget

For determining the budget of absolute angular momentum, the vertical cross section was divided into eight parts bounded by the lines $r' = 0.3$, 0.6 and 0.9, by the two side walls, the bottom, the free surface and the line $z' = 0.4$ (*cf.* Fig. 9). The derivation of the equation yielding

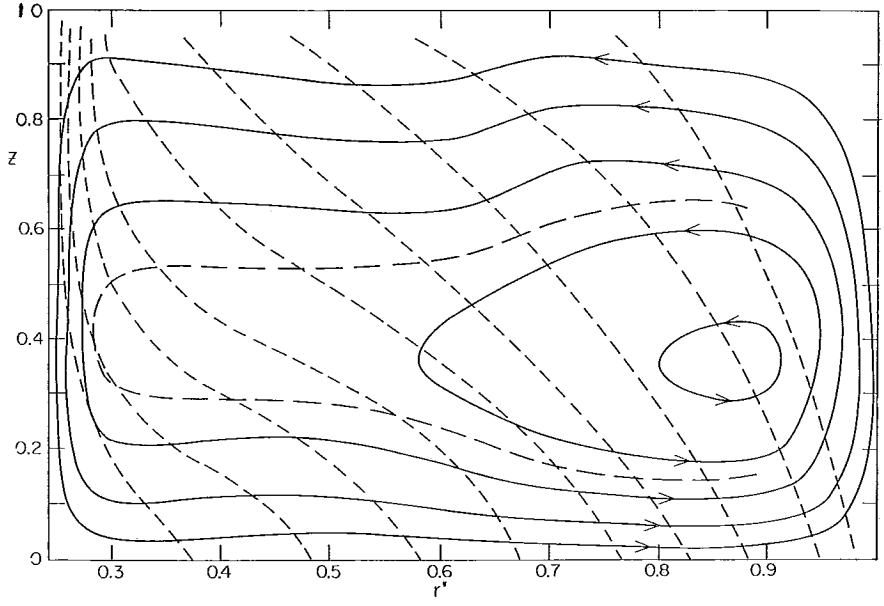

Fig. 8. Isolines of Stokes' stream function for eq. (9) and lines of constant absolute angular momentum.

a momentum budget in any of the eight compartments is well known. Equation (1) may be written as a momentum equation through multiplication by r. Assuming steady state and axial symmetry

$$rv_r \frac{\partial v_\theta}{\partial r} + v_z \frac{\partial r v_\theta}{\partial z} + v_\theta v_r + f r v_r = \frac{\partial}{\partial z}(r\tau_{\theta z}) + r\frac{\partial \tau_{\theta r}}{\partial r} + 2\tau_{r\theta}\,, \qquad (10)$$

where the density has been taken as unity.

Now:

$$\frac{1}{r}\frac{\partial}{\partial r}(v r v_\theta r^2) = v_r r \frac{\partial v_\theta}{\partial r} + v_\theta r \frac{\partial v_r}{\partial r} + 2 v_\theta v_r\,,$$

$$\frac{\partial}{\partial z}(v_\theta r v_z) = v_z \frac{\partial (v_\theta r)}{\partial z} + v_\theta r \frac{\partial v_z}{\partial z}\,,$$

so that

$$\frac{1}{r}\frac{\partial}{\partial r}(v_r v_\theta r^2) - v_\theta r \frac{\partial v_r}{\partial r} - v_\theta v_r + \frac{\partial}{\partial z}(v_z v_\theta r) - v_\theta r \frac{\partial v_z}{\partial z} + f r v_r$$

$$= \frac{\partial}{\partial z}(r\tau_{\theta z}) + r\frac{\partial \tau_{\theta r}}{\partial r} + 2\tau_{\theta r}\,. \qquad (11)$$

The equation of continuity is $\frac{\partial}{\partial r}(v_r r) + \frac{\partial}{\partial z}(v_z r) = 0$, and therefore

$$\frac{1}{r}\frac{\partial}{\partial r}(v_\theta v_r r^2) + \frac{\partial}{\partial z}(v_\theta v_z r) + f r v_r = \frac{\partial}{\partial z}(r\tau_{\theta z}) + r\frac{\partial \tau_{\theta r}}{\partial r} + 2\tau_{r\theta}\,. \qquad (12)$$

Vertical integration of (12) through a layer of depth δz (subindex u = upper, l = lower) gives

$$\frac{\delta z}{r}\frac{\partial}{\partial r}\widetilde{v_r v_\theta r^2} + v_z v_\theta r]_u - v_z v_\theta r]_l + f r \tilde{v}_r \delta z$$

$$= r[(\tau_{\theta z})_u - \tau_{\theta z})_l] + r\delta z \frac{\partial}{\partial r}\tilde{\tau}_{\theta r} + 2\delta z \tilde{\tau}_{\theta r} \qquad (13)$$

Noting that

$$\int_{r_1}^{r_2} r^2 \frac{\partial \tau_{\theta r}}{\partial r}\, dr = r^2 \tau_{\theta r}]_{r_2} - r^2 \tau_{\theta r}]_{r_1} - 2\int_{r_1}^{r_2} \tau_{\theta r} r dr \qquad (14)$$

we obtain after lateral integration from r_1 to r_2

$$\delta z\,[\widetilde{(v_r v_\theta r^2)}_{r_2} - (v_r v_\theta r^2)_{r_1}] + (\overline{v_z v_\theta}]_u - \overline{v_z v_\theta}]_l)\frac{r_2^3 - r_1^3}{3} + f\delta z \bar{\tilde{v}}_r \frac{r_2^3 - r_1^3}{3}$$

$$= (\overline{\tau}_{\theta z_u} - \overline{\tau}_{\theta z_l})\frac{r_2^3 - r_1^3}{3} + \delta z r^2 \tilde{\tau}_{\theta r}]_{r_2} - \delta z r^2 \tilde{\tau}_{\theta r}]_{r_1} \qquad (15)$$

where $\tau_{\theta z} = \nu \frac{\partial v_\theta}{\partial z}$ and $\tau_{\theta r} = \nu r \frac{\partial}{\partial r}\left(\frac{v_\theta}{r}\right)$. Here and later $\overline{\quad}$ denotes a radial average with either r^2 or r as a weighting factor depending on which is appropriate.

The Coriolis term in equation (15) is not zero in the individual compartments, but it cannot contribute to exchange at the boundaries after integration over the whole volume. On the left side, the transport terms are given by the v_θ, v_r and v_z fields previously determined. On the right side, the best measurement is that of momentum exchange at the bottom. The only terms for which there are no direct means for calculation are $\tau_{\theta z}$ at the top and $\tau_{\theta r}$ near heat and cold sources; these must be treated as residuals.

Fig. 9 shows the whole momentum budget. It is a surprising result that the fluxes through $r' = 0.9$ and the source at the bottom from $r' = 0.9$ to $r' = 1.0$ near balance, indicating that there is no momentum source

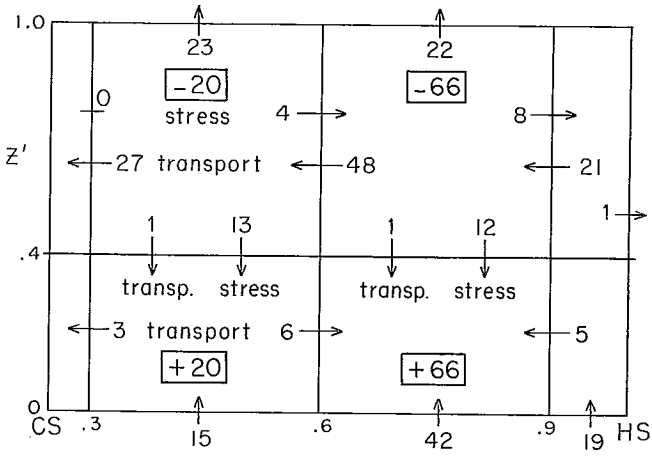

Fig. 9. Momentum budget. To be multiplied by $2\pi \times 10^{-5}$.

at the warm wall.* RIEHL and FULTZ [9] have arrived at the same conclusion for the three-wave case. The fact that the fluid ignores this potentially greatest momentum source, indicates that the structure of the general circulation is determined by factors other than boundary characteristics with respect to momentum. A surprisingly large sink is computed for the top. This checks, however, with the observation that the highest velocities occurred beneath the top, with a thin shearing layer of strong upward velocity decrease to the free surface.

We can now inquire whether the location of sinks and sources and the speed of the meridional motion in this experiment agrees with the results of ELIASSEN's model. ELIASSEN states: It is found that the meridional motion will take place mainly in the directions where the stability of the vortex is smallest, and that the speed of the meridional circulation for given sources of heat or angular momentum, will increase with decreasing stability of the vortex.

The areas of weak and strong inertial stability can be determined from Fig. 4, remembering that such stability is proportional to the gradient of absolute angular momentum. In Fig. 8 the stream function of the mass circulation and isolines of constant absolute angular momentum are shown together. The solid walls, of course, limit comparability of the experiment with atmospheric models. However, as seen from Fig. 8, the meridional motion is strongest in the lower latitudes near the free surface

* The transfer of one unit directed to this wall is within experimental error.

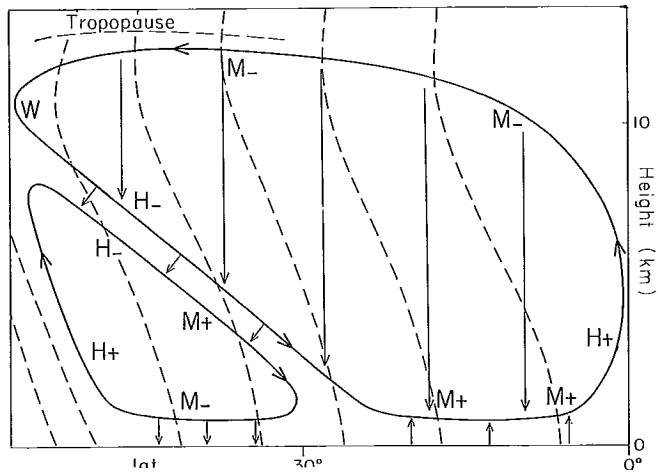

Fig. 10. Model of transverse circulation from ELIASSEN [2].

where the angular momentum gradient is weakest; and it decreases rapidly near the cold source where the momentum gradient is very large. Close to the bottom a relation is not so apparent: here also, however, the meridional motion decreases most rapidly in the region of strong momentum gradient near the heat source.

On the whole, the observations agree fairly well with ELIASSEN'S conclusions. For further comparison, Fig. 10 shows ELIASSEN'S model: it represents angular momentum and meridional circulation fields as proposed by him.

The boundary shearing stresses determined from the momentum budget will in the following be used for the computation of dissipation of kinetic energy in the boundary layers. From the kinetic energy budget it will therewith be possible to attain further information on the reliability of the momentum calculations.

Kinetic Energy Balance

Equations (1) and (2) can be transformed to energy equations by multiplying them with v_θ and v_r respectively and then adding. If v_r^2 is neglected compared to v_θ^2, and also the dissipation of meridional compared to zonal kinetic energy,

$$\frac{1}{2}\frac{dv_\theta^2}{dt} = -v_r\frac{\partial\Phi}{\partial r} + v_\theta\frac{\partial\tau_{\theta z}}{\partial z} + v_\theta\frac{\partial\tau_{\theta r}}{\partial r} + \frac{2v_\theta\tau_{\theta r}}{r}. \qquad (16)$$

Only the balance of sources and sinks over the whole volume (α) of the water will be considered. Because of the steady state and lack of transport across outer boudaries

$$\int \frac{dv_\theta^2}{dt}\, d\alpha = 0$$

and

$$0 = -\int v_r \frac{\partial \Phi}{\partial r}\, d\alpha + \int v_\theta \frac{\partial \tau_{\theta z}}{\partial z}\, d\alpha + \int v_\theta \frac{\partial \tau_{\theta z}}{\partial r}\, d\alpha + \int \frac{2 v_\theta \tau_{\theta r}}{r}\, d\alpha\,. \qquad (17)$$

The production of kinetic energy by pressure forces

$$\int v_r \frac{\partial \Phi}{\partial r}\, d\alpha = \int\int\int v_r \frac{\partial \Phi}{\partial r}\, r d\theta dr dz = 2\pi \int\int v_r \frac{\partial \Phi}{\partial r}\, r dr dz$$

$$= 2\pi D \int \widetilde{v_r \frac{\partial \Phi}{\partial r}}\, r dr = \pi D (r_c^2 - r_H^2)\, \widetilde{v_r}\, \widetilde{\frac{\partial \Phi}{\partial r}}\,, \qquad (18)$$

where D denotes the depth of the fluid, r_c the radius of the cold source and r_H the radius of the heat source. The dissipation

$$\int v_\theta \frac{\partial \tau_{\theta r}}{\partial z}\, d\alpha = \int \frac{\partial}{\partial z}(v_\theta \tau_{\theta z}) d\alpha - \int \tau_{\theta z} \frac{\partial v_\theta}{\partial z}\, d\alpha\,,$$

where the first term denotes dissipation of kinetic energy in the boundary layers and the second internal dissipation (*cf.* PALMÉN and RIEHL, [6]). Evaluation of the first term yields

$$\int \frac{\partial}{\partial z}(v_\theta \tau_{\theta z}) d\alpha = \pi D (r_c^2 - r_H^2)[\overline{v_\theta \tau_{\theta z}}_{\text{top}} - \overline{v_\theta \tau_{\theta z}}_{\text{bottom}}]\,.$$

The second term

$$\int \tau_{\theta z} \frac{\partial v_\theta}{\partial z}\, d\alpha = \nu \int \left(\frac{\partial v_\theta}{\partial z}\right)^2 d\alpha = \pi D (r_c^2 - r_H^2) \nu \widetilde{\left(\frac{\partial v_\theta}{\partial z}\right)^2}\,.$$

Similar expressions hold for dissipation of kinetic energy by lateral stresses. Since kinetic energy is very high at top and at cold wall compared to bottom and warm wall, the dissipation may be neglected in the latter two boundaries. This is in marked contrast to the atmosphere where the only boundary layer is at the ground. With these omissions equation (17) becomes

$$\widetilde{Kv_r \frac{\partial \Phi}{\partial r}} = K\overline{v_\theta \tau_{\theta z}}_{\text{top}} - 2\pi r_c D(\widetilde{v_\theta \tau_{\theta r}})_{cs} - 2\pi D(\widetilde{v_\theta^2})_{cs} - \nu K\left[\left(\widetilde{\frac{\partial v_\theta}{\partial z}}\right)^2 + \left(\widetilde{\frac{\partial v_\theta}{\partial r}}\right)^2 + \left(\widetilde{\frac{v_\theta}{r}}\right)^2\right] \tag{19}$$

where $K = \pi D(r_c^2 - r_H^2)$.

All quantities for evaluating equation (19) are known except $\tau_{\theta z})_{\text{top}}$ and $\tau_{\theta r})_{cs}$ which will now be computed from the momentum budget. The momentum transport (M_r) to the cold wall

$$M_r = \int r\tau_{\theta r} r d\theta dz = 2\pi r_c^2 \int \tau_{\theta r} dz ,$$

and the dissipation of kinetic energy through friction (F_r) near this wall

$$F_r = 2\pi r_c \int v_\theta \tau_{\theta r} dz$$

from above. These reduce to

$$M_r = 2\pi r_c^2 \nu \int \frac{\partial v_\theta}{\partial r} dz \text{ and}$$

$$F_r = \pi r_c \nu \int \frac{\partial v_\theta^2}{\partial r} dz .$$

Since the motion vanishes at the cold source $\frac{\partial v_\theta}{\partial r} = \frac{v_\theta}{r^*}$ and $\frac{\partial v_\theta^2}{\partial r} = \frac{v_\theta^2}{r^*}$ where r^* is radial distance measured from the cold wall and taken as a very small quantity. Then

$$M_r = \frac{2\pi r_c^2 \nu}{r^*} \int v_\theta dz \text{ and}$$

$$F_r = \frac{\pi r_c \nu}{r^*} \int v_\theta^2 dz .$$

The vertical wind distribution is essentially linear above the level with zero zonal motion. If a similar distribution holds close to the wall, $v_\theta' = \beta_z'$ above $z' = 0.2$, so that

$$M_r = \frac{\pi r_c^2 \nu D^2}{r^*} \beta \text{ and}$$

$$F_r = \frac{\pi r_c \nu D^3}{3r^*} \beta^2 .$$

Eliminating β from these equations,

$$F_r = \frac{M_r^2 r^*}{3\pi r_c^3 \nu D} . \tag{20}$$

The momentum transport through the top (M_z)

$$M_z = \int r \tau_{\theta z} dA$$

and the frictional dissipation in the surface layer

$$F_z = \int v_\theta \tau_{\theta z} dA$$

where A denotes area. A simple procedure for relating M_z and F_z comparable to that for M_r and F_r is not available so that one must integrate the equations numerically over small radial distances. We then obtain for the momentum transport

$$M_z = 2\pi \frac{r_2^3 - r_1^3}{3} \overline{\tau_{\theta z}}$$

and, approximately, for the kinetic energy dissipation

$$F_z = \pi(r_2^2 - r_1^2)\overline{v_\theta}\,\overline{\tau_{\theta z}} , \tag{21}$$

where correlations of v_θ and $\tau_{\theta z}$ have been omitted for small increments of radius.

Evalution of all terms in equation (19) is shown in Table 1. Within limits of computational accuracy balance is obtained; all four dissipation terms have the same magnitude.

Table 1

Evalution of equation (19) (units 10^{-3})		
	Generation	Dissipation
Generation of KE by pressure forces	2.52	
Dissipation of KE by lateral shearing stresses		0.47
Dissipation of KE by vertical shearing stresses		0.97
Dissipation of KE in surface boundary layer		0.64
Dissipation of KE at cold wall		0.33
Dissipation by $\left(\frac{v}{r}\right)^2$ term		0.36
	2.52	2.77

Potential Energy Release

One of the results of the three-wave study (3) was that the major fraction of the total release of potential energy (about twothirds) took place near both rims. Further, nearly the whole release was brought about by the ageostrophic mass circulation; the potential energy so released was used for generation of kinetic energy through pressure forces in the manner of the simple classical heat engine.

In the symmetrical experiments all potential energy transformations take place by means of the ageostrophic radial mass flow. Following RIEHL and FULTZ [8] the release (P) is given by

$$P = g\varrho_s \in \int_a T v_z d\alpha \,. \tag{22}$$

Here $\in = 2 \times 10^{-4}$ is the coefficient of thermal expansion of water and ϱ_s denotes standard density. Since there are no variations with longitude

$$P = 2\pi g \varrho_s \in \int\int T v_z r dr dz \,. \tag{23}$$

Setting $rv_z = m$ and introducing means and deviations with respect to radius,

$$P = 2\pi g \varrho_s \in \int\int [\overline{T}\,\overline{m} + \overline{(T^0 m^0)}]\, dr dz \,. \tag{24}$$

As discussed by RIEHL and FULZ [9] and PALMÉN [7] the $\overline{T}\overline{m}$ term does not contribute to kinetic energy production since it denotes mean ascent or descent over the whole cross section without tilting of isotherms. For comparison with Table 1, therefore, only the second term is of interest. If small increments of radius are considered,

$$\int \overline{T^0 m^0}\, dr = \sum_{c_s}^{H_s} T_i^0 m_i^0 \Delta r \,. \tag{25}$$

From the diagrams in this report and from measurements of vertical motion, it is apparent that practically all ascent and descent occurs within $r' = 0.01$ to 0.02 from the walls. These very small increments of radius limit the transport of heat by the mass circulation; in the narrow boundary layers the temperature gradient is large enough to obtain a satisfactory calculation of lateral heat transport by conduction, in ac-

cordance with the estimate for the heat source. Hence only an element of radius near the walls need be considered in equation (25), so that,

$$\int \overline{T^0 m^0} dr = (T_c^0 m_c^0 + T_H^0 m_H^0)\, \Delta r. \tag{26}$$

Further, since $m_c^0 + m_H^0$ may be taken as zero from the foregoing,

$$\int \overline{T^0 m^0} dr = m^0 (T_H - T_c) \Delta r\,, \tag{27}$$

and the kinetic energy producing part of the potential energy transformations, or the release of free potential energy

$$P^* = 2\pi g \varrho_s \sum \Delta r \int m^0 (T_H - T_c)\, dz. \tag{28}$$

The quantity $m = v_z r$ may be determined directly from vertical velocity measurements near heat or cold source. Alternately, v_z may be computed from the equation of continuity for which, in view of the formulation of equation (27), the incompressible form may still be used. Both of these approaches were followed, and excellent agreement was obtained in spite of the difficulties in measuring v_z in the very narrow boundary layers. Since the vertical motion takes place in such restricted portions of the volume, its magnitude is large and has the same order as v_0. Table 2 contains the pertinent quantities for evaluating equation (28), where T_H and T_c have been averaged over $\Delta r' = 0.01$.

Table 2

Evaluation of equation (28)					
z' (layer)	v_z' (cold source)	T_H	T_c	$T_H - T_c$	$(T_H - T_c)v_z'$
0.9—1.0	0.06	28.3	27.5	0.8	0.05
0.8—0.9	0.16	28.3	27.1	1.2	0.19
0.7—0.8	0.25	28.1	26.4	1.7	0.43
0.6—0.7	0.32	27.9	25.5	2.4	0.77
0.5—0.6	0.35	27.4	24.7	2.7	0.95
0.4—0.5	0.37	26.8	23.9	2.9	1.07
0.3—0.4	0.36	25.9	23.0	2.9	1.04
0.2—0.3	0.33	24.8	22.1	2.7	0.89
0.1—0.2	0.26	23.3	20.5	2.8	0.73
0 —0.1	0.11	21.6	16.5	5.1	0.55

From Table 2, $P^* = 2.59 \times 10^{-3}$, in excellent agreement with Table 1. It is seen that satisfactory and consistent results have been obtained for the entire energy cycle. Through release of free potential energy by the mass circulation, a corresponding amount of kinetic energy is produced through pressure forces. The kinetic energy so generated is dissipated internally and at the boundaries by friction for steady state. The dissipation rate must be related to the whole structure of the general circulation. From Table 1 internal dissipation is very important, in contrast to the three-wave and other cases where the Rossby number is much lower (0.2 or less compared to 1.4). In the present model a constant absolute angular momentum profile should have been achieved at the top, since there are no pressure variations with longitude. The fact that the observed jet stream speed falls far short of that demanded by the momentum principle can only be explained through action of frictional forces. It follows that at high Rossby numbers the magnitude of frictional relative to the other forces can become much greater than at low Rossby numbers. Since the jet stream and v_θ in general are in quasi-gradient equilibrium, frictional stresses and dissipation of kinetic energy influence the total temperature gradient found in the experiment outside the boundary layers.

Adknowledgment. The author is indebted to the Office of Naval Research, United States Navy, and to the Department of Meteorology, University of Chicago, for making the arrangements which permitted him to spend a year at Chicago. He also expresses his cordial thanks to Prof. H. RIEHL who has given him the kind guidance and advice throughout the work and supervised the research. Thanks are due to the whole staff of the Hydrodynamics Laboratory, Department of Meteorology, for able assistance.

REFERENCES

1. DORSEY, N. E., 1940: *Amer. Chem. Soc. Monogr.* No. 81, New York, Reinhold.
2. ELIASSEN, A. 1952: Slow thermally or frictionally controlled meridional circulations in a circular vortex. *Astrophys. Norveg.*, **5**, 60 pp.
3. FALLER, A. J., 1959: Detailed measurements in Hadley Regime symmetric convection, *Department of Meteorology, University of Chicago*, multigraphed.
4. FULTZ, D. *et al*, 1956: Studies in experimental hydrodynamics, *Final Report, Part I, Department of Meteorology, University of Chicago*, multigraphed.
5. PALMÉN, E. and K. M. NAGLER, 1948: An analysis of the wind and temperature distribution in the free atmosphere over North America in a case of approximately werterly flow. *J. Meteor.*, **5**, 58—64.
6. PALMÉN, E. and H. RIEHL, 1957: Budget of angular momentum and energy in tropical cyclones. *J. Meteor.*, **14**, 150—159.
7. PALMÉN, E., 1958: Vertical circulation and release of kinetic energy during the development of hurricane Hazel into an extratropical storm. *Tellus*, **10**, 1—23.
8. RIEHL, H. and D. FULTZ, 1957: Jet stream and long waves in a steady rotating-dishpan experiment: structure of the circulation. *Quart. J. Roy. Meteor. Soc.*, **83**, 215—231.
9. » , 1958: The general circulation in a steady rotating-dishpan experiment. *Ibid.* **84**, 389—417.